JOURNAL OF GUIDANCE, CONTROL, AND DYNAMICS
Vol. 29, No. 6, November–December 2006

Models for Rhumb-Line Attitude Maneuvers and Error Propagation Effects

Jozef C. van der Ha*
Mission Design and Operations, Columbia, Maryland 21044

DOI: 10.2514/1.18937

The attitude control of a spin-stabilized spacecraft is usually performed by a forced precession of the spin axis produced by a series of pulsed thrust actuations. A sun sensor is used for the proper timing of the thrust pulses so that the spin axis describes a rhumb-line path on the unit-sphere. The rhumb-line equations are derived from first principles and are interpreted and visualized in geometrical terms. Thruster performance parameters (i.e., the magnitude and centroid time of the thrust pulses) constitute the principal error sources governing the accuracy of the maneuver. These errors affect the total maneuver path length and its inertial heading direction, that is, the rhumb angle. An analytical model is constructed for describing the propagation of path-length and rhumb-angle errors into the resulting attitude at the conclusion of the maneuver. Detailed simulations with relevance to actual spacecraft applications have been performed to arrive at an understanding of the expected error magnification for different maneuver input parameters and initial conditions. Finally, a model is also presented for the propagation of the statistical characteristics of the input errors into the resulting error covariances of the final attitude parameters.

I. Introduction

SPIN stabilization is attractive for providing attitude pointing stability during injection maneuvers performed by solid rocket motors and bipropellant engines. This concept is used when injecting geostationary spacecraft from their transfer orbits into their operational orbits. The same approach can also be employed for the injection of a deep-space probe into its heliocentric trajectory (Farquhar et al. [1]). Because the Launcher typically delivers the spacecraft in an attitude orientation that is different from the one required for the injection maneuver there will be a need to perform attitude reorientation maneuvers. Furthermore, it may be advantageous to perform orbit corrections during the preinjection Earth phasing orbits for compensating the launch injection errors (Dunham et al. [2]). In order that the onboard thrusters are able to deliver the required $\Delta\mathbf{v}$'s, attitude maneuvers must be performed to point the spacecraft in the proper inertial directions. For instance, in the case of the CONTOUR mission, as many as 7 orbit and 12 attitude maneuvers were performed during its 6 weeks of phasing orbits (van der Ha et al. [3]).

The attitude control of a spin-stabilized spacecraft is typically performed by a forced precession of the spin axis by means of a series of pulsed thrust actuations synchronized with the spin rate. The direction of the spin axis motion can be controlled (Williams [4][†]) by introducing a delay in the thruster firings relative to the sun pulse, that is, the instant of the sun's crossing over the sun sensor's reference slit [3]. The required delay time during the maneuver is calculated on-ground and uplinked to the spacecraft along with the number of thrust pulses and their firing durations. The resulting motion of the spin axis on the unit sphere under a constant delay angle follows a rhumb-line or loxodrome path in spherical coordinates (e.g., Wertz [5], pp. 651–654).

The rhumb-line maneuver concept has been used operationally by numerous satellites since about 45 years. An overview of its original implementation on geostationary communications satellites is given in the patent of Williams [4] which dates back to April 1960. A useful model for the nutation buildup resulting from the axial thrust pulses during a rhumb-line maneuver is presented in [6].[‡]It is found that the maximum nutation angle is typically well below the one resulting from a continuous axial (orbital) maneuver.

Sierer and Snyder [7] provide an overview of the operational principles and the typical error sources relevant to the attitude determination and attitude control of spin-stabilized spacecraft based on their experiences with early communications satellites like Syncom, Early Bird, Applications Technology Satellite, and INTELSAT IIC. Furukawa [8] presents an analytical solution of the Euler equations during a precession maneuver induced by a uniform train of rectangular thrust pulses. He includes useful analytical results on the propellant expenditure, potential spin rate variations, as well as nutation effects. Hablani [9] describes a technique for designing a rhumb-line precession controller using a series of almost-periodic thrust pulses at a constant phase angle relative to the sun. He advises to control the delay angle (between the sun sensor pulse and thruster initiation) in order that any errors caused by spin variations are eliminated. Furthermore, he presents a control scheme for spacecraft with nonzero products of inertia with the objective to damp the high-frequency nutation oscillations at the conclusion of the maneuver.

Thruster performance characteristics, such as the effective magnitude and centroid time of the thrust pulse, constitute the main error sources affecting the accuracy of a rhumb-line attitude control maneuver. Inertial directional errors in the maneuver path may also be caused by timing offsets in the thrust pulses (induced, for instance, by spin rate deviations). All of these error sources modify the maneuver evolution in two independent ways, namely in terms of the total maneuver path length and in its inertial heading direction on the unit sphere. Typically, a thrust-level error leads directly to a maneuver path-length error, whereas the remaining errors predominantly affect the rhumb angle. Other maneuver errors may be induced for example by thrust vector misalignments and errors in the initial attitude knowledge but these are less significant for long maneuvers.

The paper presents a direct derivation of the rhumb-line equations from first principles and provides useful insights into the geometrical characteristics of the maneuver path within the relevant reference frames. The paper establishes a first-order analytical model for

Presented as Paper AAS-05-415 at the AAS/AIAA Astrodynamics Conference, Lake Tahoe, CA, 7–11 August 2005; received 19 July 2005; revision received 31 December 2005; accepted for publication 7 January 2006.

*Consultant; jvdha@aol.com. Senior Member AIAA.

[†]http://patft.uspto.gov/netacgi/nph-Parser?patentnumber=3758051 [cited 28 December 2005].

[‡]http://ntrs.nasa.gov/archive/nasa/casi.ntrs.nasa.gov/19660014301_1966014301.pdf [cited 28 December 2005].

predicting the propagation of errors in the thrust level and in the centroid angle of the thrust pulses into the resulting attitude pointing error at the conclusion of the maneuver. The model includes also the propagation of errors in the initial attitude estimate. Systematic simulations with practical relevance to geostationary transfer orbits and deep-space applications have been performed and the relevant results have been summarized.

II. Spin Axis Attitude Control

A. Torque Expression

Attitude control of a spin-stabilized spacecraft can be performed by one thruster (parallel to the spin axis) in a pulsed firing mode synchronized with the spin rate. However, in order to eliminate undesirable $\Delta\mathbf{v}$ effects on the orbit, an even number of balanced thrusters should be employed. Figure 1 provides an illustration of the geometrical configuration of two balanced forces $\mathbf{F}_1$ and $\mathbf{F}_2$ acting on a spacecraft spinning about its z axis with spin vector $\boldsymbol{\omega}_z$.

The torque vector $\mathbf{T}$ resulting from the forces $\mathbf{F}_j = (F_{jx}, F_{jy}, F_{jz})^T$ with associated lever arms $\mathbf{r}_j = (r_{jx}, r_{jy}, r_{jz})^T$, $j = 1, 2, \ldots, n$, may be expressed in terms of the components $(T_x, T_y, T_z)^T$ in the spacecraft body frame (x, y, z) as follows:

$$\mathbf{T} = (T_x, T_y, T_z)^T = \sum_{j=1}^{n} \{\mathbf{r}_j \times \mathbf{F}_j\}$$

with

$$T_x = \sum_{j=1}^{n} \{r_{jy}F_{jz} - r_{jz}F_{jy}\}; \qquad T_y = \sum_{j=1}^{n} \{r_{jz}F_{jx} - r_{jx}F_{jz}\}$$
$$T_z = \sum_{j=1}^{n} \{r_{jx}F_{jy} - r_{jy}F_{jx}\} \tag{1}$$

We consider a spacecraft in a pure spin (i.e., in the absence of nutation) about its major principal axis. The angular momentum vector is given by $\mathbf{H} = I_z\boldsymbol{\omega}_z$ with I_z denoting the moment of inertia and $\boldsymbol{\omega}_z$ the spin vector, both along the principal body z axis. The precession of the angular momentum vector is produced by the torque components T_x and T_y that point normal to the spin vector, whereas the component T_z leads to a change in spin rate. The spin rate ω_z is usually assumed to remain constant during the preparation of precession maneuvers, even though minor spin changes may result from thrust-level fluctuations, misalignment effects, spin inertia changes caused by propellant consumption, and by rate coupling effects inherent in the Euler equations for triaxial spacecraft (van der Ha [10]).

B. Spacecraft-Sun Frame

We introduce the instantaneous (x_S, y_S, z_S) spacecraft-sun frame defined by the spacecraft z axis (i.e., spin axis) and the sun direction represented by the unit vector $\boldsymbol{s}$ (Fig. 2). Its z_S axis is identical to the z-axis and the x_S-axis points along the intersection of the spacecraft (x, y) plane and the plane formed by the spacecraft z axis and the sun vector $\boldsymbol{s}$. The (x_S, y_S, z_S) frame can be considered frozen or quasi-inertial during the course of one spin revolution, whereas the spacecraft frame (x, y, z) in Fig. 2 rotates rapidly with the spacecraft's spin motion. The transformation matrix between the (x_S, y_S, z_S) frame and the J-2000 inertial reference frame (X, Y, Z) follows from the components z_j and s_j $(j = 1, 2, 3)$ of $\boldsymbol{z}$ and $\boldsymbol{s}$ along the inertial X, Y, Z axes (ϑ is the sun aspect angle, Fig. 2)

$$\begin{pmatrix} x_S \\ y_S \\ z_S \end{pmatrix} = \frac{1}{\sin\vartheta} \begin{bmatrix} z_1\cos\vartheta - s_1 & z_2\cos\vartheta - s_2 & z_3\cos\vartheta - s_3 \\ z_3s_2 - z_2s_3 & z_1s_3 - z_3s_1 & z_2s_1 - z_1s_2 \\ z_1\sin\vartheta & z_2\sin\vartheta & z_3\sin\vartheta \end{bmatrix} \begin{pmatrix} X \\ Y \\ Z \end{pmatrix} \tag{2}$$

The apparent singularity has no practical relevance because a rhumb-line maneuver makes no sense when the sun direction coincides with the spin axis. The spacecraft-sun frame can be considered "frozen" during each spin revolution (when assuming that the attitude change during this interval is sufficiently small). Therefore, we may apply Newton's second law within this frame to calculate the attitude change. After each spin period, we update the spacecraft-sun frame to account for the effective change of the spin axis pointing direction.

C. Precession of Angular Momentum

Newton's second law applied to rigid-body motion provides the inertial rate of change of the angular momentum $\mathbf{H}$ under the instantaneous torque vector $\mathbf{T}(t)$ acting normal to $\mathbf{H}$:

$$\mathbf{T}(t) = d\mathbf{H}/dt = \boldsymbol{\omega}_p(t) \times \mathbf{H}(t) \tag{3}$$

The instantaneous precession vector $\boldsymbol{\omega}_p(t)$ is directed normal to both the torque and angular momentum vectors and is ahead of the rotating torque vector $\mathbf{T}(t)$ by 90 deg (Fig. 3).

The torque causes the angular momentum vector $\mathbf{H}$ to precess along the vector $\Delta\mathbf{H} = \mathbf{H}(t + \Delta t) - \mathbf{H}(t) \approx \mathbf{T}(t)\Delta t$ during an infinitesimal interval Δt. In practice, the thrust interval has a finite duration $t_{on} = t_1 - t_0$ and the change in the angular momentum $\mathbf{H}$ follows by integrating Eq. (3) over the thrust interval (Fig. 4):

$$\mathbf{H}(t_1) - \mathbf{H}(t_0) = \int_{t_0}^{t_1} \mathbf{T}(t)\,\mathrm{d}t = \int_{t_0}^{t_1} \{\boldsymbol{\omega}_p(t) \times \mathbf{H}(t)\}\,\mathrm{d}t \tag{4}$$

We introduce the averaged torque and precession rate vectors $\mathbf{T}_{ave}$ and $\boldsymbol{\omega}_{ave}$ over the thrust interval $t_{on} = t_1 - t_0$:

$$\mathbf{T}_{ave} = (1/t_{on}) \int_{t_0}^{t_1} \mathbf{T}(t)\,\mathrm{d}t; \qquad \boldsymbol{\omega}_{ave} = (1/t_{on}) \int_{t_0}^{t_1} \boldsymbol{\omega}_p(t)\,\mathrm{d}t \tag{5}$$

When the change in angular momentum $\mathbf{H}$ over the thrust interval is

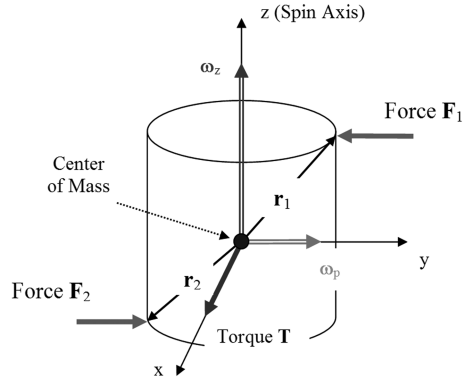

Fig. 1 Illustration of torque produced by 2 balanced thrusters.

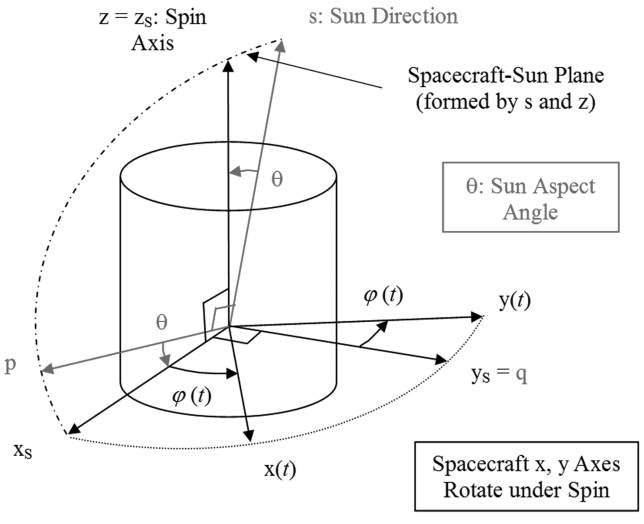

Fig. 2 Frozen spacecraft-sun frame (x_S, y_S, z_S).

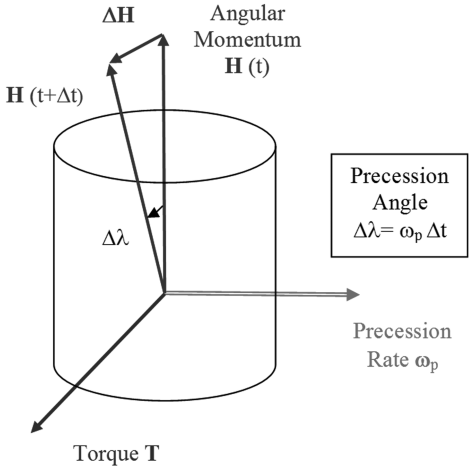

Fig. 3 Inertial precession of angular momentum vector.

sufficiently small, we can express Eq. (4) as

$$\mathbf{H}(t_1) - \mathbf{H}(t_0) = \mathbf{T}_{\text{ave}} t_{\text{on}} \approx (\boldsymbol{\omega}_{\text{ave}} \times \mathbf{H}_0) t_{\text{on}} \tag{6}$$

The vectors $\mathbf{T}_{\text{ave}}$, $\boldsymbol{\omega}_{\text{ave}}$, and $\mathbf{H}_0 = \mathbf{H}(t_0)$ are perpendicular to one another and the averaged precession rate is

$$\omega_{\text{ave}} = |\boldsymbol{\omega}_{\text{ave}}| = |\mathbf{T}_{\text{ave}}|/|\mathbf{H}_0| \tag{7}$$

The initial value $|\mathbf{H}_0|$ equals $H_0 = I_z \omega_z$ in the absence of nutation at time t_0.

D. Change in Attitude

The precession of the angular momentum $\mathbf{H}$ leads to a nutation effect whereby the instantaneous spin axis pointing direction deviates from the angular momentum vector. Analytical models [6,8] for the buildup of nutation during pulsed attitude maneuvers indicate that the maximum nutation angle remains relatively small in practice. In the case of a spacecraft spinning about its maximum inertia axis, the spin axis will align itself passively along the new angular momentum vector at the conclusion of the maneuver due to internal energy dissipation (Kaplan [11], Sec. 2.5). The alignment of the spacecraft z axis with the new angular momentum vector represents the effective change in the spacecraft attitude orientation. In the case of a spacecraft spinning about its minor axis of inertia, an active nutation control device must be employed to ensure that the spin axis pointing remains close to the angular momentum vector.

The effective change Δz in the inertial orientation of the spin axis over the thrust interval may thus be taken proportional to the change in the angular momentum vector $\mathbf{H}$ given in Eq. (6):

$$\Delta z = z(t_1) - z(t_0) \approx (\boldsymbol{\omega}_{\text{ave}} \times z_0) t_{\text{on}} \tag{8}$$

The notation Δz suggests that the change in attitude during one spin revolution may be considered infinitesimal. When using the definition of $\boldsymbol{\omega}_{\text{ave}}$ in Eqs. (5), we find

$$\Delta z = \int_{t_0}^{t_1} \{\boldsymbol{\omega}_p(t) \times z_0\}\, \mathrm{d}t \approx \int_{t_0}^{t_1} \{\omega_y(t)\mathbf{x}(t) - \omega_x(t)\mathbf{y}(t)\}\, \mathrm{d}t \tag{9}$$

The rates $\omega_x(t)$ and $\omega_y(t)$ represent the components of the precession vector $\boldsymbol{\omega}_p(t)$ along the (rotating) body unit vectors $\mathbf{x}(t)$ and $\mathbf{y}(t)$ and can be expressed in the instantaneous torque components using Eq. (3):

$$\omega_x(t) = -T_y(t)/H_0; \qquad \omega_y(t) = T_x(t)/H_0 \tag{10}$$

In the present model we assume an ideal thrust profile so that the thrust level rises instantaneously from 0 to the full force F at the time t_0 and drops back to 0 at the instant t_1. Also we assume that the thrust forces are equal for all activated thrusters and that the forces maintain a constant magnitude throughout the thrust interval (with a typical duration of at most 500 ms). These simplifying assumptions are not restrictive from a practical point of view because the thrust pulse profiles can usually be modeled fairly realistically by a representative constant thrust profile and an associated centroid time. Under the conditions of this model, the precession components $\omega_x(t)$ and $\omega_y(t)$ in Eqs. (10) remain constant throughout the thrust interval $t_{\text{on}} = t_1 - t_0$ and vanish outside this interval.

The attitude change Δz can be expressed in inertial components by using the transformation between the spacecraft body frame (x, y, z) and the spacecraft-sun frame (x_S, y_S, z_S); see Figs. 2 and 4:

$$\begin{pmatrix} x \\ y \\ z \end{pmatrix} = \begin{bmatrix} \cos\varphi(t) & \sin\varphi(t) & 0 \\ -\sin\varphi(t) & \cos\varphi(t) & 0 \\ 0 & 0 & 1 \end{bmatrix} \begin{pmatrix} x_S \\ y_S \\ z_S \end{pmatrix} \tag{11}$$

This result involves the spin phase angle $\varphi(t) = \omega_z(t - t_0)$ where t_0 represents the instant at which the two frames coincide and ω_z is the constant spin rate. The components of the attitude change along the frozen x_S and y_S axes follows now from Eq. (9):

$$\Delta z = \int_{t_0}^{t_1} \{\omega_y \cos\varphi(t) + \omega_x \sin\varphi(t)\}\mathbf{x}_S + \{\omega_y \sin\varphi(t) - \omega_x \cos\varphi(t)\}\mathbf{y}_S\, \mathrm{d}t \tag{12}$$

When introducing the centroid angle $\varphi_c = \varphi(t_c)$ for the spin phase angle relative to the x_S axis at the centroid time t_c (Fig. 4), we find the following result after explicit integration over the thrust interval (t_0, t_1):

$$\Delta z = \Delta\lambda\{\cos(\varphi_c + \tau)\mathbf{x}_S + \sin(\varphi_c + \tau)\mathbf{y}_S\} \tag{13}$$

The angle $\tau = \tan^{-1}\{T_y/T_x\}$ denotes the fixed orientation of the torque vector within the body frame (Fig. 4) and $\Delta\lambda$ is the angular path over which the attitude vector rotates under the torque produced by the thrust pulses

$$\Delta\lambda = |\Delta z| = f_g \omega_p t_{\text{on}} = f_g (T/H_0) t_{\text{on}} \tag{14}$$

The "geometric factor" $f_g = \{\sin(\varphi_{\text{on}}/2)\}/(\varphi_{\text{on}}/2)$ represents the efficiency loss caused by the extended thrust interval φ_{on} in comparison to an instantaneous impulsive pulse at the time t_c. For thrust intervals φ_{on} shorter than 90 deg, f_g is larger than 0.9. Obviously, for a very short thrust pulse (i.e., $t_{\text{on}} \to 0$) f_g approaches the value for an impulsive thrust, that is, $f_g \to 1$.

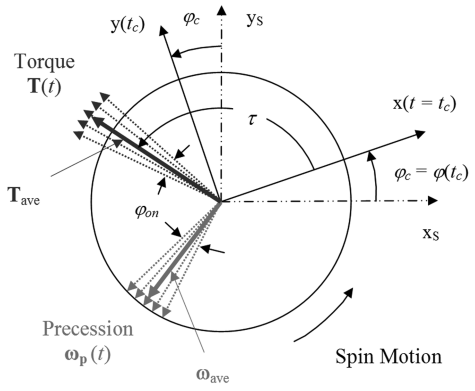

Fig. 4 Torque and precession vectors during thrust interval.

III. Rhumb-Line Attitude Maneuver

A. Rhumb Angle

Figure 2 shows the (p, q, s) frame with the p axis perpendicular to the s axis (i.e., the sun direction) within the spacecraft-sun plane (x_S, y_S). The q axis is normal to the spacecraft-sun plane and completes the triad (p, q, s):

$$\begin{pmatrix} p \\ q \\ s \end{pmatrix} = \begin{bmatrix} \cos\vartheta & 0 & \sin\vartheta \\ 0 & 1 & 0 \\ -\sin\vartheta & 0 & \cos\vartheta \end{bmatrix} \begin{pmatrix} x_S \\ y_S \\ z_S \end{pmatrix} \tag{15}$$

We introduce the heading or rhumb angle $\chi = \varphi_c + \tau - \pi/2$ and express the attitude change of Eq. (13) in terms of its components along the unit vectors $\mathbf{p}$, $\mathbf{q}$, $\mathbf{s}$:

$$\begin{aligned} \Delta z &= \Delta\lambda\{-\sin\chi\,\mathbf{x}_S + \cos\chi\,\mathbf{y}_S\} \\ &= \Delta\lambda\{-\sin\chi\cos\vartheta\,\mathbf{p} + \cos\chi\,\mathbf{q} + \sin\chi\sin\vartheta\,\mathbf{s}\} \end{aligned} \tag{16}$$

The angle ϑ is the instantaneous sun aspect angle of the attitude vector z (Fig. 2). The heading angle χ represents the direction of the attitude maneuver relative to the local sun cone (i.e., the locus of attitude vectors with constant sun aspect angles) (Fig. 5). The angles $\Delta\lambda$ and χ may be visualized as the "polar coordinates" of the attitude change Δz projected on the unit-sphere near the attitude vector z.

For illustration, we consider the case $\varphi_c + \tau = 180$ deg which is close to the geometry shown in Fig. 4. In this case, $\chi = 90$ deg and the attitude moves in the direction of the $-x_S$ axis toward the sun. In general, a heading angle of $\chi = 0$ or 180 deg represents attitude motion along the sun cone, whereas for $\chi = \pm 90$ deg the attitude moves toward or away from the sun.

The spin axis can be moved in any desired direction by selecting the appropriate centroid phase angle φ_c for the phasing of the thrust pulses. In practice (e.g., van der Ha et al. [3]), this is achieved by setting the appropriate delay for the initiation of the thrust pulses relative to the sun sensor reference pulse (i.e., the instant when the sun crosses the sun sensor meridian slit). This delay time controls the inertial direction of the torque vector and thus also the heading angle of the spin axis relative to the sun cone.

B. Rhumb-Line Geometry

When the delay angle between the initiation of the thrust pulses and the sun's reference pulse remains constant during the maneuver, the attitude vector will describe a so-called "rhumb line" on the celestial sphere (Wertz [5], pp. 651–654). In this case, the torque and precession vectors maintain fixed angles with the x_S axis of the spacecraft-sun plane (Fig. 4) so that the path of the attitude vector intersects the successive sun cones at a constant heading angle.

Figure 5 illustrates the general geometry of a rhumb-line maneuver showing the initial and final attitude vectors. The "initial sun frame" (ISF) is defined by the sun vector $\boldsymbol{s}$ and the initial attitude vector $z = z_i$ at the maneuver start time t_i. This frame is identical to the (p, q, s) frame in Fig. 2 at the time t_i. The ISF frame plays an important role in the maneuver modeling and a new designation (X_i, Y_i, Z_i) will be introduced for this frame.

The (X_i, Y_i, Z_i) frame can be considered "inertial" for all practical purposes because the apparent motion of the sun in inertial space of about 0.04 deg /hr may be considered small in view of the fact that attitude maneuvers typically have a duration of less than an hour. Thus, the error induced by the sun motion would be below 0.01 deg at the start and end of a maneuver of 0.5 hr duration (note that the sun position is taken at the midtime of the maneuver). If maneuvers of a longer duration need to be performed, the maneuver model may be broken up in a number of smaller individual maneuver legs of perhaps 10 to 30 min, each with its own sun position.

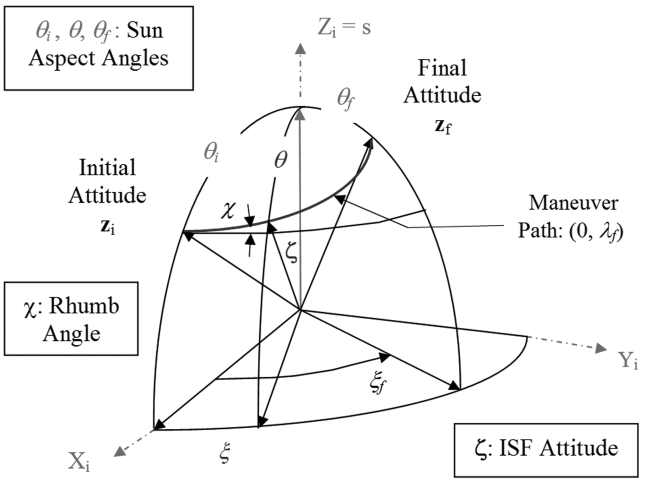

Fig. 5 Rhumb-line maneuver in initial sun frame (ISF) (X_i, Y_i, Z_i).

With the help of the transformation matrix in Eqs. (A2) and (A3) in the Appendix we can express any arbitrary attitude vector $\boldsymbol{\zeta}$ in its components in the (X_i, Y_i, Z_i) frame using the spherical coordinates ϑ and ξ (Fig. 5):

$$\boldsymbol{\zeta} = (\sin\vartheta\cos\xi, \sin\vartheta\sin\xi, \cos\vartheta)^T = [T]z = [T](z_1, z_2, z_3)^T \tag{17}$$

The sun aspect angle ϑ is associated with the vector z and ξ represents the azimuth angle of z with respect to the (X_i, Z_i) plane, that is, the plane defined by the sun vector $\boldsymbol{s}$ and the initial attitude vector z_i. For convenience and with no loss of generality, we take $\xi(t_i) = 0$ so that the components of the initial attitude vector z_i in the ISF frame are

$$\boldsymbol{\zeta}_i = (\zeta_{i1}, \zeta_{i1}, \zeta_{i3})^T = (\sin\vartheta_i, 0, \cos\vartheta_i)^T = [T]z_i \tag{18}$$

The final attitude vector $z_f = z(t_f)$ with spherical coordinates ϑ_f and ξ_f is also shown in Fig. 5.

C. Attitude Change due to Single Thrust Pulse

By differentiating Eq. (17) we can express the general attitude change $\Delta\boldsymbol{\zeta}$ after a thrust pulse in terms of the changes in the spherical angles $\Delta\vartheta$ and $\Delta\xi$ within the ISF frame:

$$\Delta\boldsymbol{\zeta} = \begin{pmatrix} \Delta\vartheta\cos\vartheta\cos\xi - \Delta\xi\sin\vartheta\sin\xi \\ \Delta\vartheta\cos\vartheta\sin\xi + \Delta\xi\sin\vartheta\cos\xi \\ -\Delta\vartheta\sin\vartheta \end{pmatrix} \tag{19}$$

The changes in the spherical angles ϑ and ξ during an attitude maneuver can be determined in explicit terms by comparison of Eq. (19) with the dynamical result in Eq. (16). This involves the transformation of the "local" (p, q, s) frame, which is attached to the instantaneous attitude vector z, into the inertial ISF reference frame

$$\begin{pmatrix} p \\ q \\ s \end{pmatrix} = \begin{bmatrix} \cos\xi & \sin\xi & 0 \\ -\sin\xi & \cos\xi & 0 \\ 0 & 0 & 1 \end{bmatrix} \begin{pmatrix} X_i \\ Y_i \\ Z_i \end{pmatrix} \tag{20}$$

The equality of the rows in Eq. (19) and the transformed components in Eq. (16) produces the relationships

$$\begin{aligned} \Delta\boldsymbol{\zeta} &= \begin{pmatrix} \Delta\vartheta\cos\vartheta\cos\xi - \Delta\xi\sin\vartheta\sin\xi \\ \Delta\vartheta\cos\vartheta\sin\xi + \Delta\xi\sin\vartheta\cos\xi \\ -\Delta\vartheta\sin\vartheta \end{pmatrix} \\ &= \Delta\lambda \begin{pmatrix} -\sin\chi\cos\vartheta\cos\xi - \cos\chi\sin\xi \\ -\sin\chi\cos\vartheta\sin\xi + \cos\chi\cos\xi \\ \sin\chi\sin\vartheta \end{pmatrix} \end{aligned} \tag{21}$$

The third row yields the functional relationship between $\Delta\vartheta$ and $\Delta\lambda$ and the first two rows can be combined to produce the connection between $\Delta\xi$ and $\Delta\lambda$:

$$\Delta\vartheta = -\Delta\lambda\sin\chi \tag{22a}$$

$$\Delta\xi = \Delta\lambda\cos\chi/\sin\vartheta \tag{22b}$$

These results express the angular changes in the spherical coordinates ϑ and ξ of the spin axis attitude in terms of the path length $\Delta\lambda$ and the rhumb angle χ which are associated with the maneuver's dynamical characteristics.

D. Attitude Change After Full Maneuver

The resulting attitude change after the full maneuver consisting of N thrust pulses will be calculated by adding the effects induced by the individual thrust pulses. When summing the contributions of Eqs. (22) for $k = 1, 2, \ldots, N$ we obtain the changes in the sun aspect angle and in the azimuth angle

$$\sum_{k=1}^{N}(\Delta\vartheta_k) = -\sum_{k=1}^{N}(\Delta\lambda_k \sin\chi_k) \tag{23a}$$

$$\sum_{k=1}^{N}(\Delta\xi_k) = \sum_{k=1}^{N}(\Delta\lambda_k \cos\chi_k / \sin\vartheta_{k-1}) \tag{23b}$$

The summation terms on the left-hand sides of Eqs. (23) are equal to the total cumulative changes in sun aspect angle and in the azimuth angle, that is, $\vartheta_f - \vartheta_i$ and $\xi_f - \xi_i$, respectively. Although Eqs. (23) allow for a varying rhumb angle throughout the maneuver, here we consider only a constant rhumb angle $\chi = \chi_k$ for $k = 1, 2, \ldots, N$. After substituting from Eq. (23a) into Eq. (23b) we can eliminate the maneuver path length $\lambda_f = \sum_{k=1}^{N}(\Delta\lambda_k)$ and obtain

$$\xi_f - \xi_i = \sum_{k=1}^{N}(\Delta\xi_k) = -\sum_{k=1}^{N}(\Delta\vartheta_k / \sin\vartheta_{k-1}) / \tan\chi \tag{24}$$

This result accommodates different individual path lengths $\Delta\lambda_k$ (for $k = 1, 2, \ldots, N$), which may be induced by variations in the thrust level over the maneuver.

The change $\Delta\vartheta_k$ in the sun aspect angle over each thruster pulse will be interpreted as infinitesimal so that Eq. (24) may be integrated over the maneuver interval

$$\begin{aligned}\xi_f - \xi_i &= \lim_{\Delta\theta\to 0}\left\{-\sum_{k=1}^{N}(\Delta\vartheta_k / \sin\vartheta_{k-1}) / \tan\chi\right\} \\ &= -\int_{\vartheta_i}^{\vartheta_f}(1/\sin\vartheta)d\vartheta / \tan\chi\end{aligned} \tag{25}$$

After performing the integration we find the familiar result for a rhumb-line maneuver [Wertz [5], p. 654, Eqs. (19–62)]:

$$y(\vartheta_f) - y(\vartheta_i) = -\tan\chi(\xi_f - \xi_i) \tag{26}$$

with the logarithmic function $y(\vartheta)$ defined by

$$y(\vartheta) = \ell_n[\tan(\vartheta/2)] \tag{27}$$

The result in Eq. (26) has the form of a straightforward linear expression between the function $y(\vartheta)$ and the azimuth angle ξ with the slope determined by the heading angle χ. The function $-y(\vartheta)$ represents a conformal mapping which is known as the Mercator projection and is widely used for mapping a spherical surface onto a flat surface (Wertz [5], p. 653). The angle χ represents the constant heading angle of the maneuver path relative to the successive solar latitude parallels (i.e., the loci of constant sun aspect angle) on the unit-sphere with the sun at its pole (Fig. 5). The slope χ is positive in case $\vartheta_i > \vartheta_f$ and negative for $\vartheta_i < \vartheta_f$.

It should be noted that the result in Eq. (26) has a mathematical singularity when the attitude vector is aligned with the sun vector (i.e., when the sun angle $\vartheta = 0$ or 180 deg). In this special case the rhumb-line model becomes indeterminate and can not be used.

E. Maneuver Path-Length

The actual maneuver path-length magnitude λ_f consists of the sum of the individual path lengths $\Delta\lambda_k$ resulting from each of the $k = 1, \ldots, N$ thruster pulses building the rhumb-line path. By direct integration of Eq. (23a) over the full range of solar aspect angles during the maneuver, we find

$$\lambda_f = \lim_{\Delta\lambda\to 0}\sum_{k=1}^{N}\{\Delta\lambda_k\} = -\int_{\vartheta_i}^{\vartheta_f}\{d\vartheta\}/\sin\chi = -(\vartheta_f - \vartheta_i)/\sin\chi \tag{28}$$

Because $\vartheta_f < \vartheta_i$ for $\sin\chi > 0$ (and vice versa), the path length λ_f is always positive. When $\chi = 0$ or 180 deg the maneuver path is along the sun cone and the result in Eq. (28) becomes singular (these cases will be addressed in Sec. V).

A rhumb-line path follows a great-circle path only when the angle χ is equal to 0, ± 90 deg, or 180 deg. In the case of a small maneuver a rhumb-line maneuver is remarkably close to a great circle in terms of path-length distance. Also for relatively large maneuvers the maneuver path lengths is usually less than 10% longer than the shortest (great-circle) distance between the initial and target attitude vectors. However, differences in respective path lengths of more than 15% can occur as well. In practical maneuver applications, the fact that a great-circle maneuver arc is shorter than a rhumb line's path length carries less weight than the rhumb line's ease of implementation.

IV. Error Propagation Model

A. Relevant Error Sources

Thruster performance and alignment characteristics constitute the principal error sources affecting the execution of an attitude maneuver, in particular:

1) Errors in the delivered thrust level
2) Offsets in the centroid time of the thruster pulses
3) Thruster mounting alignment errors
4) Thrust vector directional errors

These errors affect the maneuver execution in two ways, namely in terms of the total maneuver path length λ_f and in terms of the effective maneuver heading direction represented by the angle χ. The thrust level of noncalibrated thrusters may be off by up to 10% and act in the "along-track" direction so that the maneuver's path length is affected. The thrust-level error may be reduced to 1 to 2% by careful in-orbit calibration. On the other hand, the other error sources predominantly result in "cross-track" errors and lead to a divergence of the maneuver path from its intended direction. This corresponds to an error in the maneuver's heading direction or rhumb angle.

Another important error source (which is not addressed explicitly) originates from a deviation in the actual spin rate relative to the expected spin rate. These errors may arise from an offset in the actual initial spin rate compared with the one used in the maneuver preparation but also from unexpected spin variations occurring during the maneuver. They affect the selected delay angle between the sun sensor pulse and the initiation of the thruster firings and lead to an error in the effective rhumb angle of the maneuver path.

The model does account for estimation errors in the initial attitude z_i that propagate into the target attitude z_f.

B. Error Propagation Concept

The rhumb-line maneuver equations offer a number of intricate relationships between the variables involved. To arrive at a consistent error propagation model we must identify the independent variables as well as the associated error propagation paths. On the basis of the two different types of errors presented in the previous section, we select the maneuver path length λ (representing the thrust-level performance) and the maneuver heading angle χ (representing the effective thrust centroid time) as the fundamental independent variables affecting the maneuver performance. Additional independent variables are the initial conditions represented by the spherical position coordinates ξ_i and ϑ_i.

During the maneuver preparation, a rhumb-line path with the proper heading angle χ is determined that leads from the nominal starting attitude z_i to the desired target attitude z_f. In other words, the ISF coordinates are transformed into the final ones, that is, $(\xi_i, \vartheta_i) \to (\xi_f, \vartheta_f)$. This is accomplished by implementing the appropriate number of thruster pulses and by selecting the required

heading angle value χ. An error in either the effective thrust level or in the rhumb-angle affects the length or the direction of the maneuver, respectively. In those cases, instead of reaching the designated nominal target z_f, the maneuver will end up at a different point $z_f + \delta z_f$ on the unit sphere with ISF coordinates $(\xi_f + \delta\xi_f, \vartheta_f + \delta\vartheta_f)$. Furthermore, the initial attitude vector z_i used in the maneuver preparation may well be different from the actual attitude at the start of the maneuver; that is, $z_i = z_i + \delta z_i$ so that the initial state is actually $(\xi_i + \delta\xi_i, \vartheta_i + \delta\vartheta_i)$ instead of (ξ_i, ϑ_i).

The equations that will be employed for analyzing the error propagation over the maneuver path are taken from Eqs. (26–28) but are written in a form that emphasizes the functional dependencies

$$\vartheta_f(\lambda_f, \chi, \vartheta_i) = \vartheta_i - \lambda_f \sin\chi \tag{29a}$$

$$\xi_f(\lambda_f, \chi, \vartheta_i, \xi_i) = \xi_i - \{y(\vartheta_f) - y(\vartheta_i)\}/\tan\chi \tag{29b}$$

The function $y(\vartheta)$ stands for $\ell_n[\tan(\vartheta/2)]$. It should be noted that the dependence of ξ_f on λ_f, χ, and ϑ_i in Eq. (29b) contains "hidden" implicit terms because of the relationship $\vartheta_f = \vartheta_f(\lambda_f, \chi, \vartheta_i)$ defined by Eq. (29a).

C. Effect of Path-Length Error

The propagation of a path-length error $\delta\lambda_f$ into the final solar aspect angle ϑ_f follows from Eq. (29a):

$$\delta\vartheta_f = \{\partial\vartheta_f/\partial\lambda_f\}\delta\lambda_f \quad \text{with } \partial\vartheta_f/\partial\lambda_f = -\sin\chi \tag{30}$$

In the case when $\chi = 0$ or 180 deg, the maneuver path follows the sun cone (i.e., the latitude parallel with the sun at the pole, see Fig. 5) so that the final sun aspect angle ϑ_f is insensitive to a path-length error. On the other hand, when $\chi = \pm 90$ deg, the path moves toward or away from the sun direction and the error $\delta\vartheta_f$ will be identical in magnitude to the path-length error.

The effect of a path-length error on the resulting final azimuth angle ξ_f can be established from Eq. (29b). When accounting for the implicit dependency of ϑ_f on the path length λ_f through Eq. (29a), we find

$$\begin{aligned}\delta\xi_f &= \{\partial\xi_f/\partial y_f\}\{\partial y_f/\partial\vartheta_f\}\{\partial\vartheta_f/\partial\lambda_f\}\delta\lambda_f \\ &= \{-1/(\tan\chi)\}\{1/\sin\vartheta_f\}\{-\sin\chi\}\delta\lambda_f \\ &\rightarrow \partial\xi_f/\partial\lambda_f = \cos\chi/\sin\vartheta_f\end{aligned} \tag{31}$$

When $\chi = 0$ or 180 deg the angle ξ_f will be affected by a path-length error (Fig. 5). On the other hand, when $\chi = \pm 90$ deg the angle ξ_f will be insensitive to a path-length error. More details on these special cases will be given in Sec. V.

D. Effect of Rhumb-Angle Error

The effect of a rhumb-angle error $\delta\chi$ on the final solar aspect angle follows from Eq. (29a):

$$\delta\vartheta_f = \{\partial\vartheta_f/\partial\chi\}\delta\chi \quad \text{with } \partial\vartheta_f/\partial\chi = -\lambda_f\cos\chi \tag{32}$$

The propagation of a rhumb-angle error $\delta\chi$ into the final azimuth angle ξ_f contains an explicit as well as an implicit part and is obtained from Eq. (29b) through a chain of partial derivatives:

$$\begin{aligned}\delta\xi_f &= \{\partial\xi_f/\partial\chi\}\delta\chi + \{\partial\xi_f/\partial y_f\}\{\partial y_f/\partial\vartheta_f\}\{\partial\vartheta_f/\partial\chi\}\delta\chi \\ &= F(\lambda_f, \chi; \vartheta_i)\delta\chi\end{aligned} \tag{33a}$$

with

$$F = \lambda_f\cos^2\chi/(\sin\chi\sin\vartheta_f) + (y_f - y_i)/\sin^2\chi \tag{33b}$$

The apparent singularity in the case when $\sin\chi$ vanishes will be addressed in Sec. V.

E. Effect of Initial Attitude Error

The propagation of an error $\delta\vartheta_i$ in the initial sun aspect angle ϑ_i into the final sun angle ϑ_f is straightforward, namely $\delta\vartheta_f = \delta\vartheta_i$ because $\partial\vartheta_f/\partial\vartheta_i = 1$ from Eq. (29a). The effect of $\delta\vartheta_i$ on ξ_f can be established by a chain of partial derivatives applied to Eq. (29b):

$$\begin{aligned}\delta\xi_f &= \{\partial\xi_f/\partial y_i\}\{\partial y_i/\partial\vartheta_i\}\delta\vartheta_i \\ &+ \{\partial x_f/\partial y_f\}\{\partial y_f/\partial\vartheta_f\}\{\partial\vartheta_f/\partial\vartheta_i\}\delta\vartheta_i = G(\lambda_f, \chi; \vartheta_i)\delta\vartheta_i\end{aligned} \tag{34a}$$

with

$$G = (1/\sin\vartheta_i - 1/\sin\vartheta_f)/\tan\chi \tag{34b}$$

An error in the initial azimuth angle ξ_i does not affect ϑ_f but does have an effect on ξ_f with $\delta\xi_f = \delta\xi_i$ as can be seen from Eqs. (29).

F. Resulting Final Attitude Error

The "attitude error" refers to the angular half-cone angle (or arc-length distance on the unit sphere) between the desired target attitude unit vector z_f and the actually achieved unit vector $z_f + \delta z_f$ at the conclusion of the maneuver. In the linear or first-order error model considered here, the attitude error may be represented by the length of the attitude difference vector $|\delta z_f|$.

The attitude error can be expressed in terms of the angular errors $|\delta\vartheta_f|$ and $|\delta\xi_f|$ by means of the result of the attitude vector in terms of the ISF coordinates given in Eq. (A4) of the Appendix

$$|\delta z_f| = |\delta\boldsymbol{\zeta}_f| = \{|\delta\vartheta_f|^2 + |\delta\xi_f|^2\sin^2\vartheta_f\}^{1/2} \tag{35}$$

It is evident that the initial attitude error is given by

$$|\delta z_i| = |\delta\boldsymbol{\zeta}_i| = \{|\delta\vartheta_i|^2 + |\delta\xi_i|^2\sin^2\vartheta_i\}^{1/2} \tag{36}$$

Because all of the vectors z_i, z_f, $z_i + \delta z_f$, and $z_f + \delta z_f$ lie on the unit sphere, the difference vectors δz_i and δz_f point normal to the vectors z_i and z_f, respectively (within the linear model used here). This property can readily be confirmed in terms of the ISF coordinates, for instance by means of Eq. (21).

With the help of the results for $\delta\vartheta_f$ and $\delta\xi_f$ of Eqs. (30–34) we find

$$|\delta\vartheta_f|^2 = |\delta\vartheta_i|^2 + \sin^2\chi|\delta\lambda_f|^2 + (\lambda_f\cos\chi)^2|\delta\chi|^2 \tag{37a}$$

$$|\delta\xi_f|^2 = |\delta\xi_i|^2 + G^2|\delta\vartheta_i|^2 + (\cos\chi/\sin\vartheta_f)^2|\delta\lambda_f|^2 + F^2|\delta\chi|^2 \tag{37b}$$

With the help of these expressions, we obtain the result for the attitude error $|\delta z_f|$ from Eq. (35):

$$\begin{aligned}|\delta z_f| = \{&(1 + G^2\sin^2\vartheta_f)|\delta\vartheta_i|^2 + \sin^2\vartheta_f|\delta\xi_i|^2 + |\delta\lambda_f|^2 \\ &+ (\lambda_f^2\cos^2\chi + F^2\sin^2\vartheta_f)|\delta\chi|^2\}^{1/2}\end{aligned} \tag{38}$$

This result for $|\delta z_f|$ may be rewritten in terms of the initial attitude error $|\delta z_i|$ of Eq. (36) but remnants of the $|\delta\vartheta_i|$ and $|\delta\xi_i|$ terms will remain in the result which defeats the purpose. Furthermore, it makes good sense to use the $|\delta\vartheta_i|$ and $|\delta\xi_i|$ terms instead of $|\delta z_i|$ because of their different error characteristics. The angle ϑ_i is usually measured very accurately by a sun sensor, whereas the azimuth angle ξ_i follows from less precise Earth sensor measurements. Thus, the error $|\delta\vartheta_i|$ is significantly smaller than the error $|\delta\xi_i|$ and this distinction would be obfuscated by the use of the initial attitude error $|\delta z_i|$.

The individual dependencies of the attitude error on the four selected independent variables (when considered in isolation) are given by

$$\begin{aligned}\partial|\delta z_f|/\partial|\delta\vartheta_i| &= \{1 + G^2\sin^2\vartheta_f\}^{1/2} \\ \partial|\delta z_f|/\partial|\delta\xi_i| &= \sin\vartheta_f; \qquad \partial|\delta z_f|/\partial|\delta\lambda_f| = 1 \\ \partial|\delta z_f|/\partial|\delta\chi| &= \{\lambda_f^2\cos^2\chi + F^2\sin^2\vartheta_f\}^{1/2}\end{aligned} \tag{39}$$

The result $\partial|\delta z_f|/\partial|\delta\lambda_f| = 1$ indicates that, when the path-length

error $|\delta\lambda_f|$ is considered in isolation, it induces an error $|\delta z_f|$ in the final attitude that is identical to $|\delta\lambda_f|$ itself. This result may look odd because the length of the rhumb line between the maneuver start and end points is in general different from the corresponding great-circle arc-length distance between these two points. The apparent inconsistency originates from the inherent linearization of all error effects due to the use of only first-order differential terms. Table 1 summarizes the error propagation results.

G. Propagation of Error Statistics

The results presented above can be employed in covariance analyses for propagating the error statistics of the independent variables into the statistical properties of the achieved final attitude. In particular, if we have specific knowledge about the input error variances associated with the independent variables $\vartheta_i, \xi_i, \lambda_f$, and χ, that is

$$\begin{aligned} \sigma_{\vartheta_i}^2 &= E\{(\delta\vartheta_i)^2\}, \qquad \sigma_{\xi_i}^2 = E\{(\delta\xi_i)^2\} \\ \sigma_{\lambda_f}^2 &= E\{(\delta\lambda_f)^2\}, \qquad \sigma_{\chi}^2 = E\{(\delta\chi)^2\} \end{aligned} \tag{40}$$

we can calculate the variances at the conclusion of the maneuver by means of Eqs. (37):

$$\sigma_{\vartheta_f}^2 = E\{(\delta\vartheta_f)^2\} = \sigma_{\vartheta_i}^2 + \sin^2\chi\sigma_{\lambda_f}^2 + (\lambda_f\cos\chi)^2\sigma_{\chi}^2 \tag{41a}$$

$$\sigma_{\xi_f}^2 = E\{(\delta\xi_f)^2\} = \sigma_{\xi_i}^2 + G^2\sigma_{\vartheta_i}^2 + (\cos\chi/\sin\vartheta_f)^2\sigma_{\lambda_f}^2 + F^2\sigma_{\chi}^2 \tag{41b}$$

The formal calculation of the variance of the final attitude vector is more complicated because it involves the establishment of the three-dimensional covariance matrix of the attitude vector. This can be done most conveniently in terms of components in the ISF frame (X_i, Y_i, Z_i) in Fig. 5:

$$[\mathrm{cov}(\boldsymbol{\zeta}_f)] = E\{(\delta\boldsymbol{\zeta}_f)(\delta\boldsymbol{\zeta}_f)^T\} = \begin{pmatrix} c_{11} & c_{12} & c_{13} \\ c_{12} & c_{22} & c_{23} \\ c_{13} & c_{23} & c_{33} \end{pmatrix} \tag{42}$$

This covariance matrix may be transformed in the inertial components of the attitude vector by using the transformation matrix in Eq. (A2) of the Appendix. The error differential $\delta\boldsymbol{\zeta}_f$ in the ISF reference frame is obtained similarly as in the derivation of Eq. (21) except that $\Delta\vartheta_f$ and $\Delta\xi_f$ are now $\delta\vartheta_f$ and $\delta\xi_f$, respectively:

$$\delta\boldsymbol{\zeta}_f = \begin{pmatrix} (\cos\vartheta_f\cos\xi_f)\delta\vartheta_f - (\sin\vartheta_f\sin\xi_f)\delta\xi_f \\ (\cos\vartheta_f\sin\xi_f)\delta\vartheta_f + (\sin\vartheta_f\cos\xi_f)\delta\xi_f \\ -(\sin\vartheta_f)\delta\vartheta_f \end{pmatrix} \tag{43}$$

When assuming that the cross-correlation term $E\{(\delta\vartheta_f)(\delta\xi_f)\}$ is relatively small, the entries in the covariance matrix $[\mathrm{cov}(\boldsymbol{\zeta}_f)]$ of Eq. (42) become

$$\begin{aligned} c_{11} &= (\cos\vartheta_f\cos\xi_f)^2\sigma_{\vartheta_f}^2 + (\sin\vartheta_f\sin\xi_f)^2\sigma_{\xi_f}^2 \\ c_{22} &= (\cos\vartheta_f\sin\xi_f)^2\sigma_{\vartheta_f}^2 + (\sin\vartheta_f\cos\xi_f)^2\sigma_{\xi_f}^2 \\ c_{33} &= (\sin\vartheta_f)^2\sigma_{\vartheta_f}^2 \\ c_{12} &= \tfrac{1}{2}\sin(2\xi_f)\{(\cos\vartheta_f)^2\sigma_{\vartheta_f}^2 - (\sin\vartheta_f)^2\sigma_{\xi_f}^2\} \\ c_{13} &= -\tfrac{1}{2}\cos\xi_f\sin(2\vartheta_f)\sigma_{\vartheta_f}^2; \qquad c_{23} = -\tfrac{1}{2}\sin\xi_f\sin(2\vartheta_f)\sigma_{\vartheta_f}^2 \end{aligned} \tag{44}$$

The expected attitude covariances at the conclusion of the maneuver can be visualized as an asymmetrical cone centered about the nominal attitude pointing direction. The cone's dimensions are determined by the cross-section of the three-dimensional covariance ellipsoid with the unit-sphere. A convenient and meaningful representation of the attitude error covariance $\sigma_{\mathrm{att},f}^2$ is given by the sum of the diagonal terms of the covariance matrix:

$$\sigma_{\mathrm{att},f}^2 = \sigma_{\vartheta_f}^2 + (\sin\vartheta_f)^2\sigma_{\xi_f}^2 \tag{45}$$

The same result may be established after the diagonalization of the covariance matrix by means of a coordinate transformation into its eigenvectors with associated eigenvalues. When substituting the results of Eqs. (41) into Eqs. (45), we obtain

$$\begin{aligned} \sigma_{\mathrm{att},f}^2 = (1 + G^2\sin^2\vartheta_f)\sigma_{\vartheta_i}^2 + (\sin\vartheta_f)^2\sigma_{\xi_i}^2 + \sigma_{\lambda_f}^2 \\ + (\lambda_f^2\cos^2\chi + F^2\sin^2\vartheta_f)\sigma_{\chi}^2 \end{aligned} \tag{46}$$

The error variance $\sigma_{\vartheta_i}^2$ is usually much smaller than the variance of the other errors (because of the accurate sun sensor measurements) so that the first term on the right-hand side of Eq. (46) may be dropped in practice.

V. Special Cases

A. Maneuver Along Sun Cone

When the heading angle $\chi = 0$ or 180 deg, the maneuver path moves along the sun cone with a constant sun aspect angle ϑ_i so that ϑ_f equals ϑ_i. In general, the maneuver path will be part of a small circle (i.e., latitude parallel) with the sun as pole. In the special case when $\vartheta_i = 90$ deg, the maneuver moves along a great-circle arc. When the heading angle χ equals 0 or 180 deg, the expression in Eq. (29b) becomes indeterminate because $\tan\chi$ vanishes. This singularity originates from the integration performed in Eqs. (25) and (28) because the integrals become meaningless when the sun aspect angle ϑ stays constant.

To be able to perform error analyses for maneuvers with $\sin\chi = 0$, we need to include neighboring maneuver paths. Therefore, we allow for heading angles in the neighborhood of 0 or 180 deg with small (positive or negative) $\sin\chi = \varepsilon$ and $|\cos\chi| = 1$ with error of the order of ε^2. Equation (29a) takes now the form

$$\vartheta_f = \vartheta_i - \lambda_f\sin\chi = \vartheta_i - \varepsilon\lambda_f \tag{47}$$

By substituting this expression into Eq. (29b) we can remove the singularity identified above by applying an asymptotic expansion of the azimuth angle ξ_f in powers of ε. This procedure involves the expansion of the function $y(\vartheta_f) - y(\vartheta_i)$ of Eq. (29b) in terms of a Taylor series in powers of the small parameter $\vartheta_f - \vartheta_i = -\varepsilon\lambda_f$:

$$\begin{aligned} y(\vartheta_f) &= y_i + (\vartheta_f - \vartheta_i)\{\partial y/\partial\vartheta\}_i + \tfrac{1}{2}(\vartheta_f - \vartheta_i)^2\{\partial y/\partial\vartheta^2\}_i + \ldots \\ &= y_i - \varepsilon\lambda_f/\sin\vartheta_i - \tfrac{1}{2}(\varepsilon\lambda_f)^2\cos\vartheta_i/(\sin^2\vartheta_i) + O(\varepsilon^3) \end{aligned} \tag{48}$$

A meaningful asymptotic result for the azimuth angle ξ_f of Eq. (29b) can be established in the case when $\sin\chi \approx 0$:

$$\begin{aligned} \xi_f - \xi_i \approx (+/-)\lambda_f/\sin\vartheta_i + (+/-)\tfrac{1}{2}\varepsilon\lambda_f^2\cos\vartheta_i/\sin^2\vartheta_i \\ (\text{for } \chi \approx 0 \text{ or } 180 \text{ deg}) \end{aligned} \tag{49}$$

In the limit for $\epsilon \to 0$ the familiar result for a maneuver along the sun cone is recovered, namely $\lambda_f = |\xi_f|\sin\vartheta_i$ (Wertz [5], Eq. 19–63 on p. 654) with $\xi_f > 0$ if $\chi = 0$ and $\xi_f < 0$ if $\chi = 180$ deg.

Equations (49) allow the calculation of the error sensitivities for the cases $\chi \approx 0/180$ deg:

$$\partial\xi_f/\partial\vartheta_i \approx (-/+)\lambda_f\cos\vartheta_i/\sin^2\vartheta_i \tag{50a}$$

$$\partial\xi_f/\partial\lambda_f \approx (+/-)1/\sin\vartheta_i \tag{50b}$$

$$\partial\xi_f/\partial\chi \approx (+/-)\tfrac{1}{2}\lambda_f^2\cos\vartheta_i/\sin^2\vartheta_i \tag{50c}$$

Similar results for the error sensitivities of the final sun aspect angle ϑ_f can readily be calculated from Eq. (47). The complete list of error sensitivity results for these special cases are summarized in Table 2. For a maneuver along the sun cone, the final sun aspect angle will be insensitive to a thrust-level error (as expected from geometry) but

Table 1 Error propagations for general rhumb-line maneuver

	$\delta\vartheta_f$	$\delta\xi_f$	$\lvert\delta z_f\rvert$
$\delta\vartheta_i$	1	$G = (1/\sin\vartheta_i - 1/\sin\vartheta_f)/\tan\chi$	$\{1 + G^2\sin^2\vartheta_f\}^{1/2}$
$\delta\xi_i$	0	1	$\sin\vartheta_f$
$\delta\lambda_f$	$-\sin\chi$	$\cos\chi/\sin\vartheta_f$	1
$\delta\chi$	$-\lambda_f\cos\chi$	$F = \lambda_f\cos^2\chi/(\sin\chi\sin\vartheta_f) + (y_f - y_i)/\sin^2\chi$	$\{\lambda_f^2\cos^2\chi + F^2\sin^2\vartheta_f\}^{1/2}$

Table 2 Error propagations for rhumb-line maneuver with $\chi = 0/180$ deg

	$\delta\vartheta_f$	$\delta\xi_f$	$\lvert\delta z_f\rvert$
$\delta\vartheta_i$	1	$G = (-/+)\lambda_f\cos\vartheta_i/\sin^2\vartheta_i$	$\{1 + \lambda_f^2/\tan^2\vartheta_i\}^{1/2}$
$\delta\xi_i$	0	1	$\sin\vartheta_i$
$\delta\lambda_f$	0	$(+/-)1/\sin\vartheta_i$	1
$\delta\chi$	$-/+\lambda_f$	$F = (+/-)\frac{1}{2}\lambda_f^2\cos\vartheta_i/\sin^2\vartheta_i$	$\lambda_f\{1 + \frac{1}{4}\lambda_f^2/\tan^2\vartheta_i\}^{1/2}$

Table 3 Error propagations for rhumb-line maneuver with $|\chi| = 90$ deg

	$\delta\vartheta_f$	$\delta\xi_f$	$\lvert\delta z_f\rvert$
$\delta\vartheta_i$	1	$G = 0$	1
$\delta\xi_i$	0	1	$\sin\vartheta_f$
$\delta\lambda_f$	$(-/+)1$	0	1
$\delta\chi$	0	$F = y_f - y_i$	$\lvert y_f - y_i\rvert\sin\vartheta_f$

will be affected by a rhumb-angle error. The final azimuth angle ξ_f is of course sensitive to a path-length error.

Finally, the error covariance of the final attitude vector as defined in Eq. (45) for this special case can be written as in Eq. (46) when the specific expressions for F and G in Table 2 are substituted. An interesting special situation occurs when the initial sun angle ϑ_i is near 90 deg when both F and G may be considered negligible and a compact result for the attitude error is found:

$$\sigma^2_{\text{att},f} \approx \sigma^2_{\vartheta_i} + \sigma^2_{\xi_i} + \sigma^2_{\lambda_f} + \lambda_f^2\sigma^2_\chi \qquad (\text{for } \vartheta_i = 90 \text{ deg}) \qquad (51)$$

B. Maneuver Normal to Sun Cone

A heading angle $\chi = \pm 90$ deg means that the maneuver path is normal to the sun cone. The attitude moves toward (for $\chi = 90$ deg) or away from (for $\chi = -90$ deg) the sun position along the great meridian circle that contains all three vectors z_i, z_f, and s (Fig. 5). In these special cases, $s \cdot (z_i \times z_f)$ vanishes and this implies [Eqs. (A8) and (A9)] that the azimuth angle $\xi_f = \xi(t) = \xi_i = 0$ remains constant throughout the maneuver and the maneuver path length is now identical to the change in sun aspect angle. In the present case, there is no difficulty in using the general rhumb-line model of Eqs. (29). When substituting the specific heading angle values $\chi = \pm 90$ deg we obtain

$$\xi_f = \xi_i = 0;$$
$$\vartheta_f = \vartheta_i - \lambda_f \sin\chi = \begin{cases} \vartheta_i - \lambda_f, & \text{for } \chi = +90 \text{ deg} \\ \vartheta_i + \lambda_f, & \text{for } \chi = -90 \text{ deg} \end{cases} \qquad (52)$$

Further insight is found by considering the expressions for the initial and final attitude vectors in the ISF frame in Eqs. (17) and (18) along the meridian $\xi_i = \xi_f = 0$:

$$\boldsymbol{\zeta}_i = (\sin\vartheta_i, 0, \cos\vartheta_i)^T; \qquad \boldsymbol{\zeta}_f = (\sin\vartheta_f, 0, \cos\vartheta_f)^T \qquad (53)$$

The arc length between the vectors z_i and z_f is represented by the angle ψ_f, which in this special case is equal to the maneuver path length λ_f:

$$\lambda_f = \psi_f = \cos^{-1}(\boldsymbol{\zeta}_f \cdot \boldsymbol{\zeta}_i) = |\vartheta_f - \vartheta_i| \qquad (54)$$

The error sensitivities can readily be calculated from the results in Table 1 by substituting the specific heading angle values $\chi = \pm 90$ deg and are summarized in Table 3. Finally, the error covariance of the final attitude vector as defined in Eq. (45) for this special case can be found from Eq. (46) when substituting $G = 0$ and $F = y_f - y_i$:

$$\sigma^2_{\text{att},f} = \sigma^2_{\vartheta_i} + (\sin\vartheta_f)^2\sigma^2_{\xi_i} + \sigma^2_{\lambda_f} + (y_f - y_i)^2\sin^2_{\vartheta_f}\sigma^2_\chi \qquad (55)$$

VI. Discussion of Results

We focus on the effects of the rhumb-angle error because an error in the path length leads to an identical attitude error within the first-order linear model used here. The effect of an error in the initial attitude estimate upon the final attitude is relatively insignificant (at least for long maneuvers) and will be taken up in the statistical results below.

Figures 6–8 show the sensitivities of the final attitude coordinates to a rhumb-angle error for a number of different rhumb angles in the range from 0 to 90 deg. These results are based on simulations of an attitude maneuver of up to 180 deg long and starting with an initial sun aspect angle of 80 deg. The results for rhumb angles in different quadrants can be constructed on the basis of the underlying symmetries with the cases presented. It should be noted that the maneuvers usually terminate before reaching the terminal value of $\lambda_f = 180$ deg as is clear from Figs. 6–8. This happens in particular when the attitude vector has spiraled into the sun vector, that is, when ϑ_f reaches 0. Another reason for terminating the maneuver simulation would be when the azimuth angle ξ_f reaches 180 deg. In these cases, there is little use in continuing the simulation because there exists a shorter maneuver, namely the one with the rhumb angle 180 deg $-\chi$.

Figure 6 shows the sensitivity of the sun aspect angle to a rhumb-angle error. It shows that $\partial\vartheta_f/\partial\chi$ vanishes for a rhumb angle $\chi = 90$ deg and that the highest sensitivity occurs for a maneuver along the sun cone ($\chi = 0$). In most of the cases shown, the maneuvers terminate because the azimuth angle ξ_f reaches 180 deg. Only in the case $\chi = 90$ deg does the attitude end up along the sun vector (and for $\chi = 70$ deg it comes close). In none of the cases shown did λ_f reach 180 deg. The results in Fig. 6 are in principle valid for any initial sun aspect angle ϑ_i. However, for $\vartheta_i \neq 80$ deg,

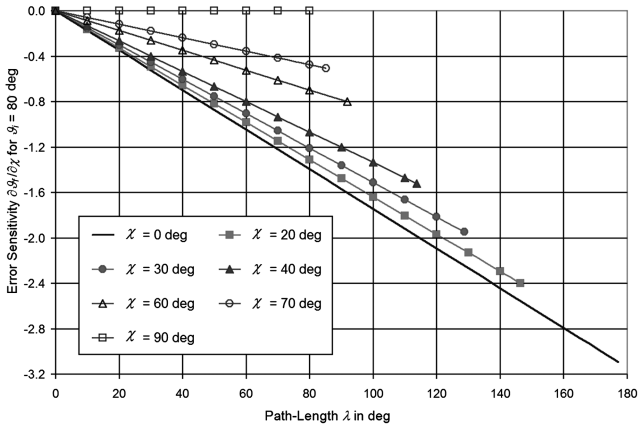

Fig. 6 Sensitivity of sun angle to rhumb-angle error $\partial\vartheta_f/\partial\chi$ for $\vartheta_i = 80$ deg.

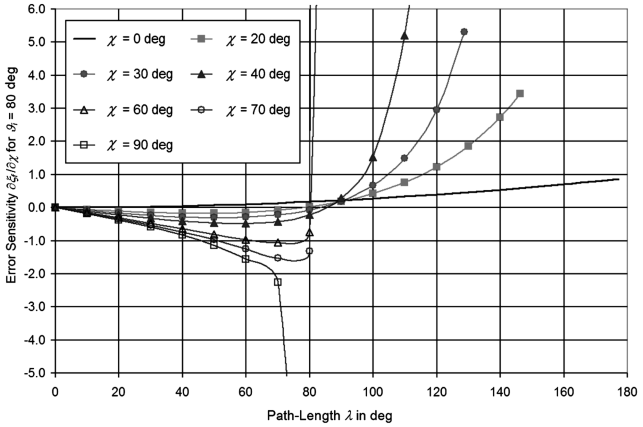

Fig. 7 Sensitivity of azimuth to rhumb-angle error $\partial\xi_f/\partial\chi$ for $\vartheta_i = 80$ deg.

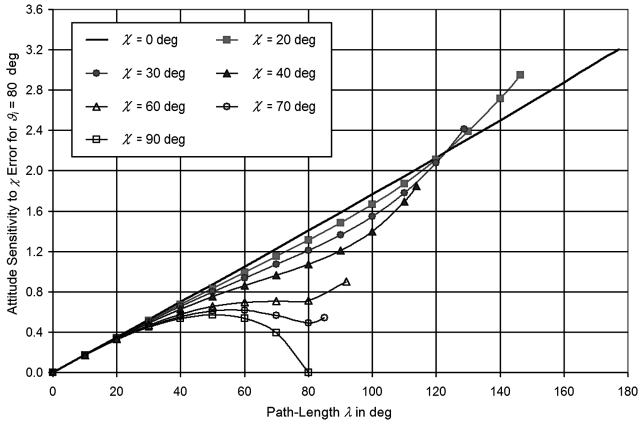

Fig. 8 Sensitivity of attitude to rhumb-angle error $\partial|\delta z_f|/\partial\chi$ (for $\vartheta_i = 80$ deg).

the maneuvers will terminate at different values of the path lengths than those shown in Fig. 6.

Figure 7 shows the sensitivity of the azimuth angle ξ_f to a rhumb-angle error for the same range of rhumb angles and for the same initial sun angle as in Fig. 6. For high rhumb angles between $\chi = 60$ deg and 90 deg, a singularity occurs due to the fact that ϑ_f approaches 0, which leads to $F \to \infty$ as can be seen from Eq. (33b). The sensitivity of the resulting attitude path to a rhumb-angle error under the same conditions is given in Fig. 8. The singularity that appeared in the results for ξ_f disappears now due to the multiplication with $\sin^2\vartheta_f$ in the entry for $\partial|\delta z_f|/\partial\chi$ in Table 1.

Figure 9 shows the sensitivity of the attitude path to a rhumb-angle error for a relatively high initial sun angle of 140 deg. In comparison with Fig. 8, the paths are generally longer because the bulge of the unit sphere near sun angle values of 90 deg needs to be crossed (in most cases). There are two paths (i.e., $\chi = 30$ deg and 40 deg) in Fig. 9 that manage to reach the end point $\lambda_f = 180$ deg before hitting $\xi_f = 180$ deg or $\vartheta_f = 0$ (the latter occurs only for $\chi = 90$ deg).

Table 4 summarizes the results of the sensitivity factor $\partial|\delta z_f|/\partial\chi$ describing the propagation of a given rhumb-angle error into the resulting attitude error for a number of rhumb angles and initial sun angles ϑ_i within the range from 30 to 150 deg. Figures 8 and 9 illustrate that maneuvers may terminate before reaching the final end point $\lambda_f = 180$ deg, namely when ξ_f reaches 180 deg or $\vartheta_f \to 0$. This obviously happens more frequently when the initial sun angle is small because the path toward $\xi_f = 180$ deg is relatively short and the sun is near as well. These are the principal reasons for the more benign error magnifications in the upper right corner of Table 4.

Table 4 shows that higher values of the initial sun angle in the lower half of the Table lead in general to higher attitude errors than corresponding rhumb angles with lower values of ϑ_i. This is caused by the fact that only rhumb angles in the range from 0 to 90 deg are considered in Table 4 so that the maneuver path typically crosses the bulge of the unit sphere for initial sun angles $\vartheta_i > 90$ deg and these paths will typically be relatively long. Table 4 is useful for establishing an estimate of the upper bound for the attitude error resulting from a particular maneuver with given rhumb angle and initial sun aspect angle. For instance, it predicts that the magnification of a rhumb-angle error into an attitude error is at most about 3.9 for any meaningful maneuver with initial sun angle ϑ_i within the range 30 to 150 deg (which is valid for essentially all spacecraft).

Finally, Table 5 illustrates the practical application of the statistical propagation model. On the basis of given input errors we calculate the resulting error statistics of the attitude at the conclusion of the maneuver. The maneuver considered in Table 5 has a length of 180 deg with initial and final sun angles $\vartheta_i = 124$ deg and $\vartheta_f = 56$ deg and rhumb-angle $\chi = 21.8$ deg. This type of maneuver was actually performed for CONTOUR (van der Ha et al. [3]). The inputs used in Table 5 are the (worst-case or 3-σ level) error variances σ_{ϑ_i} and σ_{ξ_i} for the initial attitude position together with the variances σ_λ and σ_χ for the maneuver path length and the rhumb-angle errors. The latter two inputs can be calculated from the specified thrust-level performances and the expected errors in the thrust centroid times. Offsets in the delay angle (between sun sensor pulse and thrust pulse initiation) caused for instance by spin rate errors should also be incorporated in σ_χ. The outputs are given in terms of the variances of the sun aspect angle, the azimuth angle and the attitude vector at the conclusion of the maneuver as predicted by the covariance propagations in Eqs. (41) and (46).

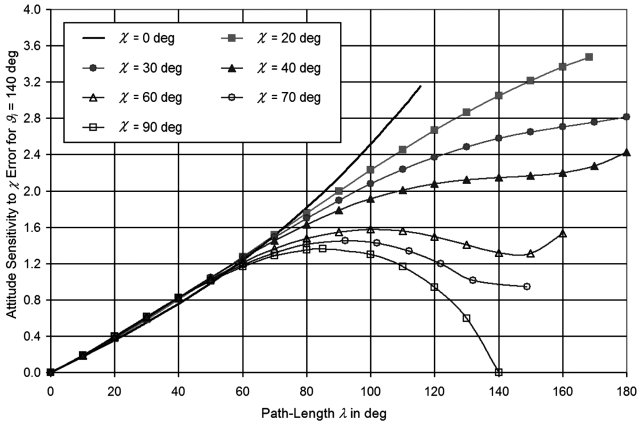

Fig. 9 Sensitivity of attitude to rhumb-angle error $\partial|\delta z_f|/\partial\chi$ (for $\vartheta_i = 140$ deg).

Table 4 Maximum rhumb-angle error propagation to attitude error ($\lambda_f, \xi_f < 180$ deg)

χ:	0 deg	10 deg	20 deg	30 deg	40 deg	50 deg	60 deg	70 deg	80 deg	90 deg
$\vartheta_i = 30$ deg	2.65	1.93	1.40	1.01	0.73	0.51	0.34	0.22	0.20	0.20
40 deg	3.16	2.44	1.82	1.34	0.97	0.68	0.45	0.29	0.27	0.26
50 deg	3.42	2.84	2.20	1.64	1.20	0.85	0.57	0.37	0.34	0.33
60 deg	3.46	3.11	2.52	1.93	1.43	1.01	0.68	0.45	0.42	0.41
70 deg	3.35	3.25	2.77	2.19	1.64	1.18	0.79	0.53	0.50	0.49
80 deg	3.21	3.26	2.95	2.41	1.85	1.34	0.90	0.62	0.58	0.57
90 deg	π	3.19	3.04	2.60	2.04	1.49	1.01	0.72	0.68	0.66
100 deg	3.21	3.11	3.05	2.73	2.20	1.64	1.12	0.82	0.78	0.76
110 deg	3.35	3.13	3.00	2.79	2.34	1.78	1.23	0.94	0.89	0.88
120 deg	3.46	3.30	2.95	2.80	2.45	1.91	1.34	1.08	1.03	1.01
130 deg	3.42	3.54	3.12	2.72	2.50	2.02	1.44	1.25	1.19	1.17
140 deg	3.16	3.67	3.47	2.81	2.43	2.10	1.58	1.45	1.38	1.36
150 deg	2.65	3.47	3.86	3.24	2.52	2.11	1.87	1.72	1.64	1.62

Table 5 Worst-case error statistics for a 180 deg maneuver before and after calibration

Case	Inputs				Outputs		
#	σ_{ϑ_i}	σ_{ξ_i}	σ_λ	σ_χ	σ_{ϑ_f}	σ_{ξ_f}	$\sigma_{\text{att},f}$
Before calibration of thrust level and centroid time							
1	0.1 deg	0	0	0	0.1 deg	0	0.1 deg
2	0	3 deg	0	0	0	3 deg	2.49 deg
3	0	0	18 deg	0	6.7 deg	20.1 deg	18.0 deg
4	0	0	0	5 deg	14.6 deg	1.7 deg	14.7 deg
5	0	0	18 deg	5 deg	16.0 deg	20.2 deg	23.2 deg
6	0.1 deg	3 deg	18 deg	5 deg	16.0 deg	20.4 deg	23.3 deg
After calibration of thrust level and centroid time							
3c	0	0	5.4 deg	0	2.0 deg	6.0 deg	5.4 deg
4c	0	0	0	1 deg	2.9 deg	0.3 deg	2.9 deg
5c	0	0	5.4 deg	1 deg	3.5 deg	6.0 deg	6.1 deg
6c	0.1 deg	3 deg	5.4 deg	1 deg	3.5 deg	6.8 deg	6.6 deg

The upper part of Table 5 uses inputs that have not been calibrated, that is, a worst-case thrust-level error of 10% of the path length and a worst-case rhumb-angle error of 5 deg are taken. The initial sun angle is produced by a sun sensor and is relatively accurate whereas the initial azimuth angle is measured by a (noncalibrated) Earth sensor. The results indicate that the final attitude may be off by more than 23 deg from the desired target attitude. Such a large pointing error is typically considered unacceptable in view of system design constraints (e.g., telecommunications). The lower part of Table 5 shows similar results but uses (mildly) calibrated thrust-level and centroid times. The worst-case path-length error is now assumed to be 3% and the rhumb-angle error is 1 deg. It follows that the resulting attitude error is reduced by a factor 3 to 4 and will more likely be considered acceptable.

VII. Conclusion

The equations describing rhumb-line attitude maneuvers for spinning satellites have been derived from first principles and have been interpreted and visualized in geometrical terms. The paper establishes first-order analytical models for describing the propagation of errors in the effective thrust-level and in the effective centroid angle of the thrust pulses into the resulting attitude pointing error at the conclusion of the maneuver. The models include the effects of initial attitude estimation errors on the final attitude pointing. Systematic simulations have been performed and the results have been summarized in graphical as well as tabular forms.

Appendix: Rhumb-Line Geometry

I. Initial Sun Frame and Inertial Coordinates

The ISF with axes (X_i, Y_i, Z_i) is defined in Fig. 5 by the sun vector $\boldsymbol{s}$ and the initial attitude vector $\boldsymbol{z}_i$. The unit vectors along the (X_i, Y_i, Z_i) axes can be expanded in components along the J-2000 inertial axes (X, Y, Z) with the help of the known vectors $\boldsymbol{z}_i$ and $\boldsymbol{s}$:

$$\mathbf{X}_i = (\boldsymbol{z}_i - \cos\vartheta_i \boldsymbol{s})/\sin\vartheta_i; \qquad \mathbf{Y}_i = (\boldsymbol{s}\times\boldsymbol{z}_i)/|\boldsymbol{s}\times\boldsymbol{z}_i| \qquad \mathbf{Z}_i = \boldsymbol{s} \tag{A1}$$

where ϑ_i represents the sun aspect angle associated with the initial attitude vector $\boldsymbol{z}_i$. After expressing $\boldsymbol{z}_i$ and $\boldsymbol{s}$ in their inertial coordinates $(z_{i1}, z_{i2}, z_{i3})^T$ and $(s_1, s_2, s_3)^T$, respectively, the formal coordinate transformation between the two reference frames can be written as

$$\begin{pmatrix} X_i \\ Y_i \\ Z_i \end{pmatrix} = \frac{1}{\sin\vartheta_i}\begin{bmatrix} z_{i1} - s_1\cos\vartheta_i & z_{i2} - s_2\cos\vartheta_i & z_{i3} - s_3\cos\vartheta_i \\ z_{i3}s_2 - z_{i2}s_3 & z_{i1}s_3 - z_{i3}s_1 & z_{i2}s_1 - z_{i1}s_2 \\ s_1\sin\vartheta_i & s_2\sin\vartheta_i & s_3\sin\vartheta_i \end{bmatrix}\begin{pmatrix} X \\ Y \\ Z \end{pmatrix} \tag{A2}$$

The orthonormal transformation matrix (A2) is written as $[T]$ with entries $T_{jk}(j, k = 1, 2, 3)$ and the inverse transformation is $[T]^{-1} = [T]^T$. The matrix inversion is meaningful because the initial sun angle is nonzero in practice. To distinguish between the ISF and inertial coordinates of the attitude vector $\boldsymbol{z}$, the ISF components of the attitude vector is written as $\boldsymbol{\zeta} = (\zeta_1, \zeta_2, \zeta_3)^T$, so that we have from Eq. (A2):

$$\boldsymbol{\zeta} = (\zeta_1, \zeta_2, \zeta_3)^T = [T](z_1, z_2, z_3)^T = [T]\boldsymbol{z} \tag{A3}$$

II. Attitude in Initial Sun Frame

The expansion of an arbitrary attitude vector in terms of its ISF components was given in Eq. (17) so that the final attitude vector $\boldsymbol{z}_f$ can be expressed in ISF coordinates as

$$\boldsymbol{\zeta}_f = (\zeta_{f1}, \zeta_{f2}, \zeta_{f3})^T = (\sin\vartheta_f \cos\xi_f, \sin\vartheta_f \sin\xi_f, \cos\vartheta_f)^T \quad \text{(A4)}$$

The calculation of the angles ϑ_f and ξ_f from the target attitude vector $\boldsymbol{z}_f$ follows from (A3) and (A4):

$$\vartheta_f = \cos^{-1}(\zeta_{f3}) = \cos^{-1}(\boldsymbol{s} \cdot \boldsymbol{z}_f) \quad \text{(A5a)}$$

$$\xi_f = \tan^{-1}(\zeta_{f2}/\zeta_{f1}) = \tan^{-1}\{[(\boldsymbol{s} \times \boldsymbol{z}_i) \cdot \boldsymbol{z}_f]/[(\boldsymbol{z}_i - \cos\vartheta_i \boldsymbol{s}) \cdot \boldsymbol{z}_f]\} \quad \text{(A5b)}$$

These relationships allow the calculation of the angular coordinates (ϑ_f, ξ_f) in the initial sun frame from the known initial attitude vector $\boldsymbol{z}_i$ and the specified target attitude vector $\boldsymbol{z}_f$. Also the calculation of the required rhumb angle χ from the specified initial and target attitude vectors with the help of Eq. (26) makes use of the angles (ϑ_f, ξ_f).

The inverse transformation from a given set (ϑ_f, ξ_f) coordinates to the inertial components of the attitude vector $\boldsymbol{z}_f$ makes use of Eq. (A4) to obtain the components $\boldsymbol{\zeta}_f = (\zeta_{f1}, \zeta_{f2}, \zeta_{f3})^T$ in the initial sun frame. This is then followed by the inverse transformation of Eq. (A3) to obtain the associated inertial vector $\boldsymbol{z}_f = (z_{f1}, z_{f2}, z_{f3})^T$.

III. Geometrical Relationships

The denominator in Eq. (A5b) can be simplified with the help of the arc-length angle $\psi_f = \cos^{-1}(\boldsymbol{z}_i \cdot \boldsymbol{z}_f)$ between the initial and target attitude vectors $\boldsymbol{z}_i$ and $\boldsymbol{z}_f$:

$$(\boldsymbol{z}_i - \cos\vartheta_i \boldsymbol{s}) \cdot \boldsymbol{z}_f = \cos\psi_f - \cos\vartheta_i \cos\vartheta_f \quad \text{(A6)}$$

Spherical geometry in the triangle formed by the vectors $\boldsymbol{s}$, $\boldsymbol{z}_i$, and $\boldsymbol{z}_f$ in Fig. 5 provides a relationship between the arc-length angle ψ_f and the azimuth angle ξ_f:

$$\cos\psi_f = \cos\vartheta_i \cos\vartheta_f + \sin\vartheta_i \sin\vartheta_f \cos\xi_f \quad \text{(A7)}$$

Also the following remarkable set of relationships can be established by spherical geometry in the same triangle:

$$(\boldsymbol{s} \times \boldsymbol{z}_i) \cdot \boldsymbol{z}_f = (\boldsymbol{z}_f \times \boldsymbol{s}) \cdot \boldsymbol{z}_i = (\boldsymbol{z}_i \times \boldsymbol{z}_f) \cdot \boldsymbol{s} = \sin\vartheta_i \sin\vartheta_f \sin\xi_f \quad \text{(A8)}$$

Equations (A7) and (A8) provide a confirmation of the result for ξ_f in Eq. (A5b):

$$\begin{aligned} \sin\xi_f &= \{(\boldsymbol{s} \times \boldsymbol{z}_i) \cdot \boldsymbol{z}_f\}/(\sin\vartheta_i \sin\vartheta_f) \\ \cos\xi_f &= (\boldsymbol{z}_i - \cos\vartheta_i \boldsymbol{s}) \cdot \boldsymbol{z}_f/(\sin\vartheta_i \sin\vartheta_f) \end{aligned} \quad \text{(A9)}$$

These expressions indicate again that the rhumb-line model looses its validity when ϑ_i or ϑ_f vanishes which occurs when one of the attitude vectors is aligned with the sun vector.

REFERENCES

[1] Farquhar, R. W., and Dunham, D., "The Indirect Launch Mode: A New Launch Technique for Interplanetary Missions," *Acta Astronautica*, Vol. 45, No. 4, 1999, pp. 491–497.

[2] Dunham, D. W., Muhonen, D. P., Farquhar, R. W., Holdridge, M., and Reynolds, E., "Design and Implementation of CONTOUR's Phasing Orbits," Paper AAS 03-208, 2003; *Advances in the Astronautical Sciences*, edited by D. J. Scheeres, M. E. Pittelkau, R. J. Proulx, and L. A. Cangahuala, Univelt, Inc., San Diego, CA, 2003, Vol. 114, Pt. 3, pp. 1535–1548.

[3] van der Ha, J., Rogers, G., Dellinger, W., and Stratton, J., "CONTOUR Phasing Orbits: Attitude Determination & Control Concepts and Flight Results," Paper AAS 03-150, 2003; *Advances in the Astronautical Sciences*, edited by D. J. Scheeres, M. E. Pittelkau, R. J. Proulx, and L. A. Cangahuala, Univelt, Inc., San Diego, CA, 2003, Vol. 114, Pt. 2, pp. 767–781.

[4] Williams, Donald D., "Velocity Control and Orientation of a Spin-Stabilized Body," U.S. Patent 3,758,051, filed April 18, 1960.

[5] Williams, R. S., "Gas Jet Maneuvers," *Spacecraft Attitude Determination and Control*, edited by Wertz, J. R., Sec. 19.3, Reidel, Dordrecht, The Netherlands, 1978.

[6] Anon., "Advanced Syncom: Summary Report," Vol. 1, Hughes Aircraft Company SSD 31118R; NASA Contract No. 5-2797, 31 October 1963, pp. 4.10–4.18.

[7] Sierer, W. H., and Snyder, W. A., "Attitude Determination and Control of Syncom, Early Bird, and Applications Technology Satellites," *Journal of Spacecraft and Rockets*, Vol. 6, No. 2, Feb. 1969, pp. 162–166.

[8] Furukawa, M., "Precession Maneuver Performed by Applying a Uniform Train of Thrust Pulses," *Journal of Spacecraft and Rockets*, Vol. 13, No. 10, October 1976, pp. 600–604.

[9] Hablani, H. B., "Interplanetary Spacecraft Controller Using Thrusters," *Journal of Guidance, Control, and Dynamics*, Vol. 21, No. 4, July–August 1998, pp. 542–550.

[10] van der Ha, J. C., "Perturbation Solution of Attitude Motion Under Body-Fixed Torques," *Acta Astronautica*, Vol. 12, No. 10, October 1985, pp. 861–869.

[11] Kaplan, *Modern Spacecraft Dynamics and Control*, John Wiley & Sons, New York, NY, 1976.